IEEE Access
Multidisciplinary | Rapid Review | Open Access Journal

Received October 2, 2018, accepted October 12, 2018, date of publication October 16, 2018,
date of current version November 19, 2018.

Digital Object Identifier 10.1109/ACCESS.2018.2876435

Modeling of Piercing Based on DEFORM-3D and the Ensemble OSC-PLS-ELM Method

DONG XIAO[1,2], FENGHUA YANG[1,2], BA TUAN LE[1,2,3], AND SHENGYONG ZHANG[1,2]

[1]Information Science and Engineering School, Northeastern University, Shenyang 110819, China
[2]Intelligent Mine Research Center, Northeastern University, Shenyang 110819, China
[3]College of Control Technology, Le Quy Don Technical University, Hanoi 100000, Vietnam

Corresponding author: Dong Xiao (xiaodong@ise.neu.edu.cn)

This work was supported in part by the National Natural Science Foundation of China under Grant 61733003, Grant 41371437, Grant 61203214, Grant 61473072, Grant 61773105, and Grant 61374147, in part by the Fundamental Research Funds for the Central Universities, China, under Grant N150402001 and Grant N160404008, in part by the National Key Research and Development Plan, China, under Grant 2016YFC0801602, and in part by the National Twelfth Five-Year Plan for Science and Technology Support, China, under Grant 2015BAB15B01.

ABSTRACT The seamless tube, being widely used in the automobile, aviation, petroleum, chemical, building, boiler, and military industries, is called the ''blood vessel of industry.'' The demands for high-quality seamless tubes are increasing continuously. Piercing is the first deformation process in seamless tube production and has great influence on the quality of the product. This paper takes the Diescher piercer as the object of study and builds the DEFORM finite-element model of piercing process. The DEFORM model of piercing process can substitute for practical production and serve as a simulation platform of the production process. The DEFORM model can be used for the optimization of the process parameters and the prediction of quality, and it also greatly reduces the debugging time and the production cost. Therefore, the model has great theoretical significance and is of great value in practical use. Finally, by combining the DEFORM finite-element model with the ensemble OSC-PLS-ELM mathematical model, we build the hybrid model, which further increases the precision of the quality forecast. The ensemble OSC-PLS-ELM method has the advantages of both the PLS and ELM, i.e., the characteristics of robustness and feature extraction of the PLS method and the quick nonlinear processing capability of ELM.

INDEX TERMS Data models, ELM (extreme learning machine); seamless Tube, DEFORM-3D, hybrid modeling.

I. INTRODUCTION

Seamless tubes are referred to as industrial blood vessels. Seamless tubes are widely used in a variety of fields, such as automobile, aviation, petroleum, chemical, architectural, boiler and military industries. With the rapid development of the economy, the requirements for product quality also become increasingly high. At each phase, the production of seamless tubes is tightly monitored and controlled. Waste products or substandard products can be produced at any phase if such deficiencies are not detected in time. As a consequence, the process may result in energy waste and a low utilization rate during production procedures [1]–[3].

The three deformation processes in the production of seamless tubes are piercing, tube rolling and reducing. Tube piercing is the first deformation process in the production process of hot rolled seamless tubes. The Mannesmann piercing unit consists of two barrel-shaped rolls, two guide discs and one plug, as shown in Figure 1. The quality of the tube hollow and the process variables are more complicated for this process because it is a multistage, complex nonlinear, and dynamic multivariable batch process. Furthermore, because of the continuity of the production process and the limitations

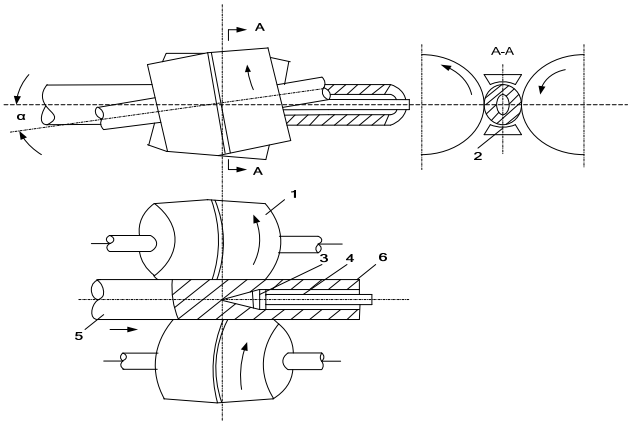

1-Roll; 2- Guide disc; 3-Plug; 4- Plug bar; 5- Tube blank; 6- Tube

FIGURE 1. Drawing of Piercer.

on monitoring instruments, it is quite difficult to measure the quality of the tube hollow in a timely manner in practice. The quality control is achieved by the staged random sampling through the workers' regulation of the processing parameters based on their experience. Certain relations between the processing parameters and the quality information, such as tube hollow deformation, twist, inner and outer cracks and surplus strain, have been determined by some scholars based on the element method [4]–[6]; however, it was found to be difficult to link the processing parameters and quality parameters one by one. Based on the BP neural network method, the relation model between tube hollow qualities and the processing parameters, e.g., roller shape, feed angle, and plug advance, had been built by reference [7]; however, the accuracy of the quality model was relatively low because of the limitations on modeling method and processing parameters. The authors of references [8]–[10] had built the relation model based on the MPLS method; however, relatively low accuracy of the quality model was obtained because of the limitations of the linear method.

The shape of tube rolling tool is complicated, and the movement of the deformation tool includes both rotation movement and linear movement. The external force the tool bears includes the front tension and the back tension besides the external force of rolls, guide discs and plugs. There are many factors that influence the piercing process, including the roll, the plug, the guide disc, the feed angle, the toe angle, the cone angle of the inlet, and the cone angle of the outlet. These factors make the analysis of the geometry, the mechanics and the kinematics of the deformation space of the tube rolling process very complicated. Therefore, developing a method to accurately determine the parameters during piercing is a crucial problem that remains to be solved in the design and production of seamless tubes.

Obtaining appropriate process parameters of cross piercing is crucial in smoothly completing the piercing process of a seamless tube and guaranteeing the quality of shell to be pierced. In the cross-piercing process of the tube, the metal deformation is very complicated, and it is difficult to measure the metal flow. In practical production, engineers often depend on their experience or draw on the experience of the unit of the same type to select the parameters of the piercing process; thus, it is difficult to guarantee the highest quality of the shell. Using optimized parameters in the model for simulation can avoid the need for debugging the optimized parameters in the production site and reduce unnecessary losses. Therefore, building a three-dimensional model of the piercer to simulate the piercing process is of great theoretical importance and practical significance. However, the precision of DEFORM-3D cannot satisfy the requirements of production very well. To address this issue, the ensemble OSC-ELM-PLS algorithm is proposed. Compared with single PLS and single ELM, the proposed algorithm has the advantages of both the specialties of robustness and specialty extraction of PLS method and the quick nonlinear processing capability of ELM. Based on the DEFORM-3D model, we utilize the ensemble OSC-ELM-PLS algorithm to build the hybrid model using practical data. The precision of the hybrid model is higher than that of the individual DERORM-3D and data-driven models.

The main contributions in this paper are highlighted below.

1) We establish the DEFORM-3D model of the piercing process based on the actual production.

2) We propose an ensemble OSC-ELM-PLS modeling algorithm that has the characteristics of robustness and feature extraction of the PLS method and the quick nonlinear processing capability of ELM.

3) We build the hybrid model by combining the DEFORM-3D and ensemble OSC-ELM-PLS methods.

II. BUILDING OF FINITE ELEMENT MODEL OF PIERCING PROCESS

The finite element method is an effective numerical computing method. DEFORM (Design Environment for Forming) is a finite element analysis software suite that was developed by the Battle Columbus Laboratory of America at the beginning of the 1980s [11]–[14]. DEFORM is a set of Finite Element Method (FEM) models based on the processing simulation system that is applicable for hot, cold and warm forming analog simulations and is specially designed and used for analyzing the three-dimensional flow of materials and the temperature during the production of all forms of metals. The objects that DEFORM considers are complicated three-dimensional parts, the die, etc., and the typical application of DEFORM includes the forging, extruding, heading, rolling, hammer forging, bending and other forming processes. The practical production will benefit greatly from the process data

A. THE SELECTION OF TUBE BLANK SIZE AND MATERIAL

In consideration of the actual situation of the site, the computing power and the computing time of the computer used in the practical production, the specification of the tube blank that is selected and used for analog computation is the following: the diameter Db=178 mm; the material is AISI-1045, which is similar to 45# steel in Chinese grade steel. When determining the length of the round tube blank, it is necessary to guarantee that the rolled piece fills the deformation area. To reduce the unevenness of the wall thickness, the centering hole is set at the bitten end of the tube blank, the depth of centering hole is h=10 mm, and the diameter is d=30 mm.

B. BUILDING OF GEOMETRIC MODEL

The helical groove of skew rolling of the solid tube blank is formed by the rolls and the guide discs. The main size, the rotating speed and the adjustment parameters of the deformation tool are as follows: the diameter of the roll Dg=1000 mm; the cone angle of the inlet $\beta = 2.75°$; the rotational speed ng=120 r/min; the diameter of the guide disc Dp=1800 mm; the rotational speed np=26 r/min; the feed angle $\alpha = 12°$; the toe angle $\Phi = 0°$; the distance between the rolls Bck=154.6 mm; the distance between the guide discs Lck=173 mm.

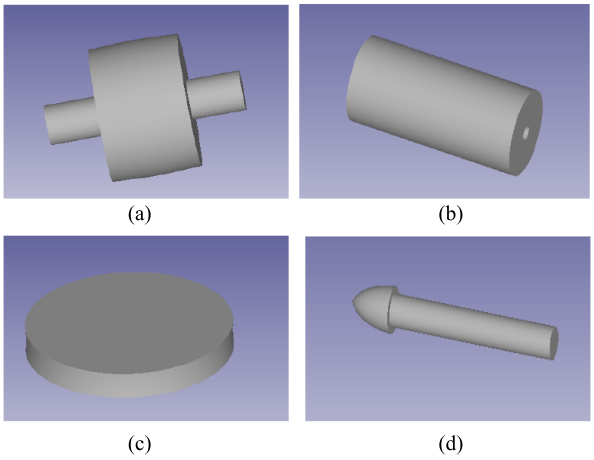

FIGURE 2. Drawing of parts of Piercer.

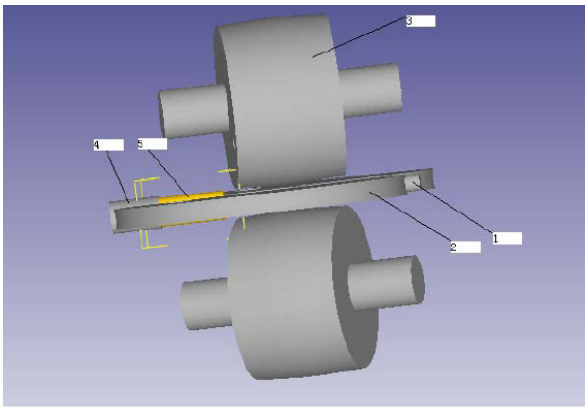

1- Plug; 2- guide disc; 3- Roll; 4- Plug bar; 5-Tube

FIGURE 3. Three-dimensional model of piercing.

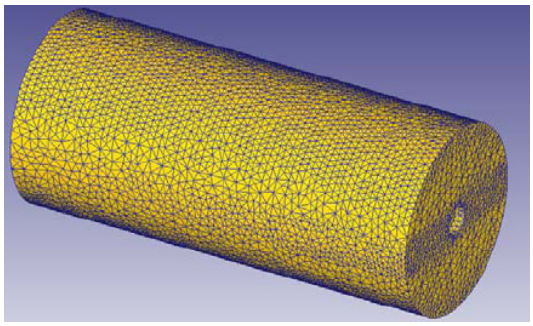

FIGURE 4. Grid division drawing of tube blank.

The roll, the guide disc and the plug are regarded as the dies in the simulation. The geometric models of the roll, the guide disc and the plug are built according to the size and specifications used in the production of the seamless tube factory of BAOSTEEL. Their three-dimensional graphics are shown in Figure 2.

To obtain an almost identical situation of the production site during the course of simulation, the pushing bar (its function is approximately equal to the function of the pusher in the production) is adopted to push the tube blank into the cavity bore in the bitten stage of the tube blank. A pushing bar is also installed at the tail end of the plug; the main function of the pushing bar in the stimulation is to put the rolled shell on it to avoid bending of the shell caused by the rotation when it is rolled. Because the deformations of the roll, the guide disc and the plug are extremely small compared to the tube blank in the piercing process, they can be ignored and set as the rigid body in the simulation. However, to consider the heat exchange between the roll, guide disc and plug and the tube blank in the temperature simulation, the necessary grids are also divided in those dies. Because Deform-3D software does not have the appropriate functionality to build the die, Pro/E, the three-dimensional modeling software, is adopted to build the real dies. According to the schematic diagram of piercing shown in Fig. 1, we build the three-dimensional model shown in Figure 3.

C. DETERMINATION OF INITIAL AND BOUNDARY CONDITION

1) SELECTION AND DIVISION OF TUBE BLANK UNIT

Three aspects should be considered for the selection of the length of the tube blank and the quantity of division of grids: a) the length of tube blank can guarantee that the tube blank can fill the deformation zone and be rolled steadily; b) the blank can be produced in actual production. Taking these two aspects into account, after many tests and selections, the following were determined: the final length of the tube blank is 550 mm, and the divided grids are 60,000 grids; these results are shown in Figure 4.

2) MECHANICS BOUNDARY

The coefficients of friction between the tube blank and the die are basically the same. The coefficient between the roll and the tube blank is 0.4. The coefficient between the guide disc and the tube blank is 0.3. The coefficient between the plug and the tube blank is 0.3.

3) TEMPERATURE BOUNDARY

The blooming temperature of the tube blank is 1200°C, and the working temperature of the roll is 150°C; the initial temperature of the guide disc is set to 100°C, and the initial temperature of the plug is set to 100°C.

4) CONDITION OF MOVEMENT

The rotating speed of the roll and the guide disc is set according to the rotating speed of practical production. After the tube blank is bitten, driven by the frictional force between the roll and the guide disc, the tube blank is rolled to complete the finite element simulation of the piercing process. Except for the head and tail of rolled piece, the deformation of the rolled piece in the whole piercing process can be regarded as a steady-state deformation.

D. DETERMINATION OF INITIAL AND BOUNDARY CONDITION

First, we utilize the front processor of DEFORM to set all the necessary parameters according to the given actual parameters of the roll, the guide disc and the pushing bar of

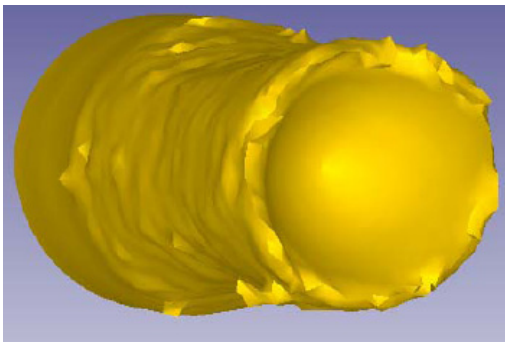

FIGURE 5. The tube blank in the piercing process.

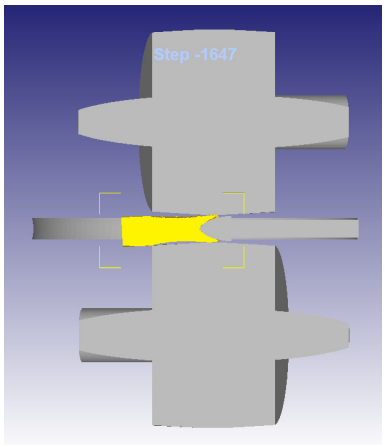

FIGURE 6. The section view of piercing process.

the piercer. Second, DEFORM generates the database, simulates the whole piercing process and finds its solution. Finally, DEFORM simulates the piercing process in the postprocessor. Figures 5-6 show pictures of the simulation process and the data monitoring in the piercing process.

III. HYBRID MODELING METHOD FOR THE PIERCING QUALITY PREDICTION

To improve the quality prediction accuracy of the DEFORM-3D model, a hybrid modeling method is proposed. The hybrid modeling method is conducted by combining the DEFORM-3D modeling method with the Ensemble OSC-PLS-ELM data modeling method. The DEFORM model is the foundation of the entire hybrid model. When conducting the DEFORM modeling, it is necessary to propose the rational simplifying hypothesis on the object; otherwise, the modeling will become extremely complicated. Those hypotheses generally lead to the inaccuracy of the model. In addition, some actions of the external disturbance of the process can also change continuously and are also difficult to accurately describe. These factors result in the certain deviation of the DEFORM model from the practical model. To identify this deviation, it is necessary to utilize the Ensemble OSC-PLS-ELM data model to modify the DEFORM model. The Ensemble OSC-PLS-ELM data model

TABLE 1. Modeling variable table for the first unsteady piercing phase.

NO	Variables	The mean of variables
1	x_{11}	upper roll reduction
2	x_{12}	lower roll reduction
3	x_{13}	upper roll angle
4	x_{14}	lower roll angle
5	x_{15}	the rev of upper roll
6	x_{16}	the rev of lower roll
7	x_{17}	the position of pusher
8	x_{18}	the position of mandrel thrust block
9	x_{19}	the position of mandrel

is superimposed on the DEFORM model via the compensation of the model error. The output of DEFORM modeling and the output of the ELM network jointly form the final output of the model [41]. The modeling process is shown in Figure 7.

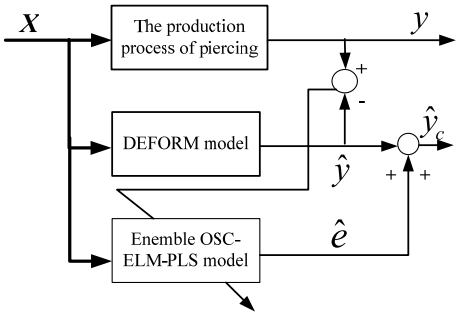

FIGURE 7. Structural drawing of hybrid Model.

A. ANALYSIS ON THE FACTORS THAT AFFECT TUBE HOLLOW QUALITY

The billet piercing process could be primarily separated into three phases: the first unsteady piercing phase, the steady piercing phase and the second unsteady piercing phase. By analyzing the technical feature, the variables at different stages will exert different effects on the tube hollow quality. The variables of each stage are shown in Table 1, Table 2 and Table 3.

For quality evaluation, quantitative index of the tube hollow quality is needed [15]. It can be obtained by off-line measurement. The transversal thickness unevenness is the ratio of the maximum thickness deviation to the nominal thickness and can be calculated as formula (1).

$$\Delta S\% = \frac{\delta_{\max} - \delta_{\min}}{\delta_{\mathrm{HOM}}} \times 100 \tag{1}$$

Where, $\Delta S\%$—the relative transversal thickness unevenness;
$\delta_{\max}$ — the maximum tube wall thickness;
$\delta_{\min}$ — the minimum tube wall thickness;
δ_{HOM} — the nominal tube wall thickness.

TABLE 2. Modeling variable table for the steady piercing phase.

NO	Variables	The mean of variables
1	x_{21}	upper roll reduction
2	x_{22}	lower roll reduction
3	x_{23}	upper roll angle
4	x_{24}	lower roll angle
5	x_{25}	the rev of upper roll
6	x_{26}	the rev of lower roll
7	x_{27}	the position of pusher
8	x_{28}	rev of left guide disc
9	x_{29}	rev of left guide disc

TABLE 3. Modeling variable table for the second unsteady piercing phase.

NO	Variables	The mean of variables
1	x_{31}	upper roll reduction
2	x_{32}	lower roll reduction
3	x_{33}	upper roll angle
4	x_{34}	lower roll angle
5	x_{35}	the rev of upper roll
6	x_{36}	the rev of lower roll
7	x_{37}	rev of left guide disc
8	x_{38}	Rev of left guide disc

The longitudinal thickness unevenness is the differential value between the mean value of the front-end tube wall thickness and the back-end tube wall thickness. It can be calculated as formula (2).

$$\Delta S_{np} = \frac{\sum_{i=1}^{n} \delta_{nep}}{n} - \frac{\sum_{i=1}^{n} \delta_{3an}}{n} \tag{2}$$

Where, $\sum_{i=1}^{n} \delta_{nep}$ and $\sum_{i=1}^{n} \delta_{3an}$ are the measured sum of tube wall thickness. n is the sum of points measured [16].

B. ORTHOGONAL SIGNAL CORRECTION (OSC) ALGORITHM

Many high-frequency noises are sandwiched into collecting production data. It will reduce the modeling accuracy. So the original data preprocessing is very necessary. Based on the introduction of Wold's OSC method [17]–[21], several other OSC algorithms have been proposed and we also use this algorithm in this paper. The basic idea is filtering irrelevant information about Y by letting X is a vector in the direction orthogonal to Y before the establishment of model. We summarized them below in our own words:

(1) Center and scale the data to give the raw matrices X and Y;

(2) Compute the first principal component (PC_1) from a PCA of X and let t0 be the PC_1;

(3) Orthogonalize t_0 to Y: $t_{new} = (I\text{-}Y(Y^TY)^{-1}Y^T)t_0$;

(4) Compute the PLS weight vector, w, that satisfies $X_w = t_{new}$;

(5) Compute a new score vector t0 from X and w: $t_0 = X_w$;

(6) Repeat steps (3), (4), and (5) until t_0 has converged;

(7) Compute a loading vector p_0: $p_0 = X^Tt_0/\ t_0^Tt_0$;

(8) Subtract the correction form X to obtain the residuals X_{OSC}: $X_{OSC} = X - t_0p_0^T$.

C. NONLINEAR PLS

Wold et al. extended the PLS method to the nonlinear field [22], [23]

(1) *External Relation Model:*

$$X = TP^T + E = \sum_{a=1}^{A} t_a p_a^T + E$$
$$Y = UQ^T + F = \sum_{a=1}^{A} u_a q_a^T + F \tag{3}$$

(2) *Internal Relation Model:*

$$\hat{u}_a = f\ (t_a) + \varepsilon \tag{4}$$

where $f\ (\cdot)$ is the nonlinear function, and ε is the residual.

The nonlinear PLS method, in which the internal model adopts the neural network, has gained extensive application because the neural network has the capability of fitting nonlinear behavior [24].

D. ELM ALGORITHM

In supervised batch learning, a finite number of input-output samples for training are used [25]–[29]. For N arbitrary distinct samples $(x_i, t_i) \in R^n \times R^m$ (where x_i is an $n \times 1$ input vector, and t_i is an $m \times 1$ target vector), if a with $\tilde{N}$ hidden nodes SLFN (single-hidden layer feed forward neural network [30]–[34]) can approximate these N samples with no error, it then signifies that there exist β_i, a_i and b_i such that

$$f_{\tilde{N}}\left(x_j\right) = \sum_{i=1}^{\tilde{N}} \beta_i G\left(a_i, b_i, x_j\right) + \varepsilon_j = t_j \tag{5}$$

where $j = 1, \ldots, N$, a_i and b_i are the learning parameters of the hidden nodes that are randomly selected on the basis of the proof given by Huang et al.;β_i is the weight linking the ith hidden node to the output node;$G\ (a_i, b_i, x)$ is the output of the ith hidden node with respect to the input x; and $\tilde{N}$ is the number of hidden nodes [35]–[40]. Thus, equation (5) can be written compactly as

$$H\beta = T \tag{6}$$

Equation (6) then becomes a linear system, and the output weights β are estimated by

$$\tilde{\beta} = H^+T \tag{7}$$

E. ENSEMBLE OF OSC-PLS-ELM ALGORITHM

Ensemble OSC-PLS-ELM contains many OSC-PLS-ELM networks with the same number of hidden nodes, and each network has the same activation function for each hidden node. P networks are constructed in the ensemble of OSC-PLS-ELM. All P OSC-PLS-ELM networks are trained with new data in each incremental step. The input parameters for each OSC-PLS-ELM networks are randomly generated, and the output weights are obtained analytically on the basis of the sequentially arrived input data. By calculating the average of the outputs of each OSC-PLS-ELM network, the final output of the OSC-PLS-ELM network is obtained. Assume the output of each OSC-PLS-ELM network is $g^j(x_i)$, $j = 1, 2, \ldots P$. Hence, we have

$$g(x_i) = \frac{1}{P}\sum_{i=1}^{P} g^j(x_i) \tag{8}$$

F. ENSEMBLE OF OSC-PLS-ELM MODELING STEPS

The difference between the nonlinear PLS modeling method based on ELM and the linear PLS method is that the former one uses ELM to establish the internal nonlinear model and update the internal and external models at the same time. The linear external model is reserved, the attributive information of process through PLS is extracted, the collinearity of data is eliminated, and the dimension of input variable reduced by using this method; moreover, it introduces ELM to build nonlinear internal model between input score vector matrix and output score vector, and improves the nonlinear processing capability of internal model. Therefore, compared with single PLS and single ELM, OSC-PLS-ELM has the advantages of both—the specialties of robustness and specialty extraction of the PLS method and the quick nonlinear processing capability of ELM.

The modeling and testing steps of the Ensemble OSC-PLS-ELM are given below:

(1) Distribute two standardized data matrix, $X \in R^{n\times m}$ and $Y \in R^{n\times p}$, Y is the model errors between the DEFORM model and the actual quality value X is

$$\boldsymbol{X} = [\boldsymbol{x}_1, \boldsymbol{x}_2, \cdots \boldsymbol{x}_p] \tag{9}$$

(2) Process the data using the OSC algorithm.

(3) Configure the batch data of the batch process, use the cross-validation method to determine the number of latent variables, and use the linear PLS method to compute the score vector matrix T and U and load vector matrix P and Q for modeling sample X and Y.

$$\begin{aligned} X &= TP^T + E = \sum_{a=1}^{A} t_a p_a^T + E \\ Y &= UQ^T + F = \sum_{a=1}^{A} u_a q_a^T + F \end{aligned} \tag{10}$$

(4) Distribute the node number of the ELM hidden layer and activation function, use ELM to establish the nonlinear model between internal models T, U, and obtain $U = f_{ELM}(T)$, where $f_{ELM}(\cdot)$ is the nonlinear function indicated by ELM.

(5) After new batch data X_1, Y_1 are obtained, first perform PLS decomposition, and then obtain the score vectors and the load vectors T_1, U_1, P_1, Q_1.

$$\begin{aligned} X_1 &= T_1 P_1^T + E \\ Y_1 &= U_1 Q_1^T + F \end{aligned} \tag{11}$$

(6) Check the accuracy of the model by using test data. Conduct PLS decomposition on the test data X_2 and obtain score vector T_2.

$$X_2 = T_2 P^T + E \tag{12}$$

Introduce T_2 into the Ensemble OSC-PLS-ELM model, calculate $U_2 = f_{OSC-PLS-ELM}(T_2)$, and then obtain the model prediction through $\hat{Y} = UQ^T$. The modeling process is shown in Figure 8.

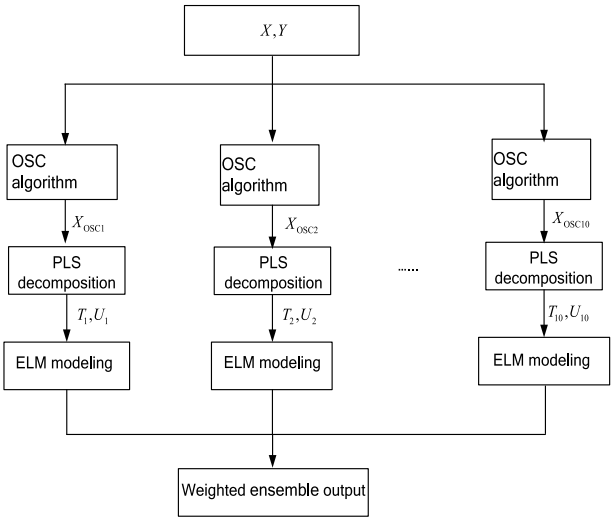

FIGURE 8. Frame chart of ensemble OSC-PLS-ELM algorithm.

IV. SIMULATION AND EXPERIMENT

To verify the accuracy of the method, 30 piercing tubes of the Diescher Mannesmann piercer from the seamless tube factory of the Baosteel Company produced in January 2014 are selected in this paper. The modeling variables are shown in Table 1. The first 20 shells are used to establish the quality prediction model. The prediction results are shown in Figure 9. Utilize the same process parameters to establish the DEFORM model of the piercing process. A hybrid model is built on the strength of the data of the actual process and of the DEFORM model. The last 10 shells are used for testing the hybrid model. The generalization results are shown in Figure 10.

As shown in Figure 9, the prediction accuracy of the transverse wall thickness of the piercing quality model of the hybrid model, Deform model and MPLS model are 93.51%, 91.81 and 91.93%, respectively. As shown in Figure 10, the

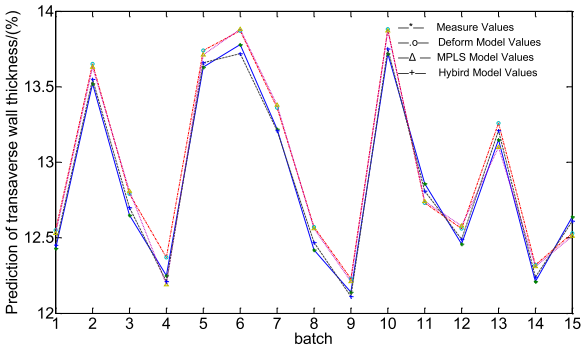

FIGURE 9. Prediction result of transverse wall thickness of quality model.

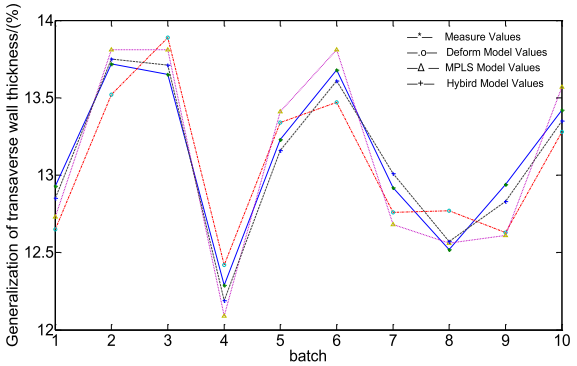

FIGURE 10. Generalization result of transverse wall thickness of quality model.

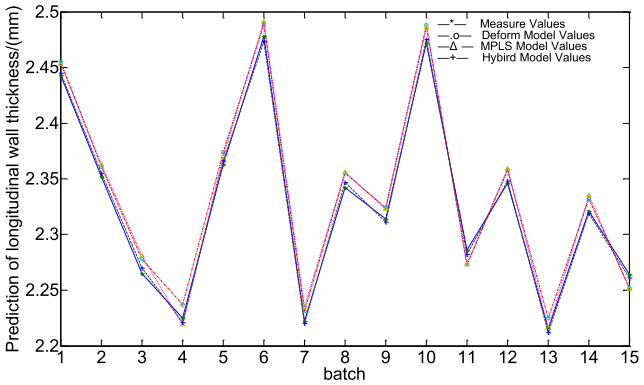

FIGURE 11. Prediction result of longitudinal wall thickness of quality model.

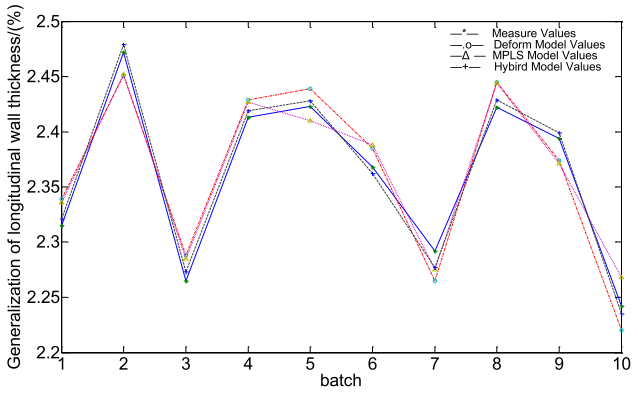

FIGURE 12. Generalization result of longitudinal wall thickness of quality model.

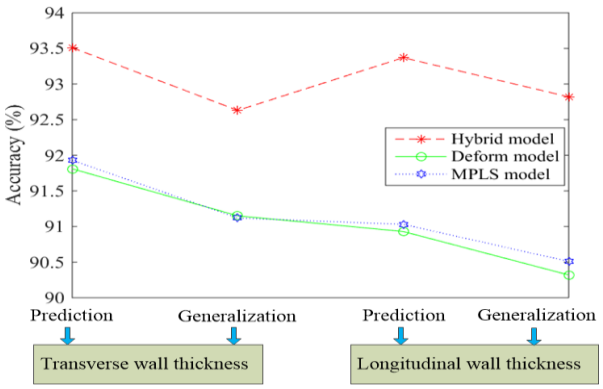

FIGURE 13. Comparison of different models.

TABLE 4. Comparison of the piercing quality models.

Method of modeling	Transverse wall thickness		Longitudinal wall thickness	
	Prediction Accuracy	Generalization Accuracy	Prediction Accuracy	Generalization Accuracy
Hybrid model	93.51	92.63	93.37	92.82
Deform model	91.81	91.15	90.93	90.32
MPLS model	91.93	91.12	91.03	90.51

generalization accuracy of transverse wall thickness of the piercing quality model of the hybrid model, Deform model and MPLS model are 92.63%, 91.15 and 91.21%, respectively. As shown in Figure 11, the prediction accuracy of the longitudinal wall thickness of the piercing quality model of the hybrid model, Deform model and MPLS model are 93.37%, 90.93 and 91.03%, respectively.

As shown in Figure 12, the generalization accuracy of the longitudinal wall thickness of the piercing quality model of the hybrid model, Deform model and MPLS model are 92.82%, 90.32 and 90.51%, respectively. The comparison results among the three different piercing quality models are displayed in Table 4 and Figure 13.

V. CONCLUSION

This paper presented a study of the quality modeling of piercing. First, the DEFORM-3D model was built to optimize the process parameters and the prediction of piercing quality. Next, to improve the accuracy of quality prediction, the ensemble OSC-PLS-ELM method was proposed for correcting the DEFORM-3D model. Finally, the feasibility and validity of the modeling method based on the hybrid model was proved via the simulation and experiment results; the proposed hybrid model was found to be more accurate

than the individual DEFORM-3D and data-driven models. Moreover, the hybrid model can be extended to the quality prediction of other batch processes.

ACKNOWLEDGMENT

Note to Practitioners: In this paper, a hybrid model is proposed for the quality prediction of a seamless tube. The model includes the DERORM-3D model and the ensemble OSC-PLS-ELM model. The ensemble OSC-PLS-ELM model is used to correct the error of the DERORM-3D model. The proposed approach significantly improves the prediction accuracy of the model. Experimental results show the performance of the approach. The approach can be used not only in quality prediction of seamless tube but also in many other important industrial processes.

REFERENCES

[1] L. S. Li, *Plastic Deformation Theory of Steel Tubes*. Beijing, China: Metallurgical Industry Press of China, 1985, pp. 82–84.
[2] N. Abedrabbo, R. Mayer, A. Thompson, C. Salisbury, M. Worswick, and I. van Riemsdijk, "Crash response of advanced high-strength steel tubes: Experiment and model," *Int. J. Impact Eng.*, vol. 36, no. 8, pp. 1044–1057, Aug. 2009.
[3] X.-F. Ding, Y.-H. Shuang, Q.-Z. Liu, and C.-J. Zhao, "New rotary piercing process for an AZ31 magnesium alloy seamless tube," *Mater. Sci. Technol.*, vol. 34, no. 4, pp. 408–418, 2018.
[4] H. Naoi, N. Kitakami, M. Mizumura, and Y. Kuriyama, "Study of intrusion bending for steel tubes with thin wall thickness," *J. Mater. Eng. Perform.*, vol. 17, no. 3, pp. 376–381, Jun. 2008.
[5] S. Urbanski and J. Kazanecki, "Assessment of the strain distribution in the rotary piercing process by the finite element method," *J. Mater. Process. Technol.*, vol. 45, nos. 1–4, pp. 335–340, 1994.
[6] Y. Wang, X. D. Qian, J. Y. R. Liew, and M.-H. Zhang, "A numerical and theoretical investigation on composite pipe-in-pipe structure under impact," *Steel Compos. Struct.*, vol. 22, no. 5, pp. 1085–1114, Dec. 2016.
[7] M. Zeinoddini, G. A. R. Parke, and J. E. Harding, "Interface forces in laterally impacted steel tubes," *Exp. Mech.*, vol. 48, no. 3, pp. 265–280, Jun. 2008.
[8] X. Dong, P. Xiaoli, M. Zhizhong, J. Minxing, and W. Fuli, "Quality prediction of tube hollow based on step-by-step staged MICR," *Chin. J. Sci. Instrum.*, vol. 28, no. 12, pp. 2190–2196, 2007.
[9] D. Xiao, X.-L. Wang, X.-L. Pan, and Z.-Z. Mao, "Quality prediction and control of tube hollow," *J. Central South Univ. Technol.*, vol. 18, no. 3, pp. 767–772, 2011.
[10] X.-L. Pan, D. Xiao, Z.-Z. Mao, Y.-Q. Chang, and F.-L. Wang, "Quality prediction of tube hollow based on mean value staged MPLS," *J. Syst. Simul.*, vol. 20, no. 7, pp. 1677–1680, 2008.
[11] M. A. Fakih, S. Mustapha, J. Tarraf, G. Ayoub, and R. Hamade, "Detection and assessment of flaws in friction stir welded joints using ultrasonic guided waves: Experimental and finite element analysis," *Mech. Syst. Signal Process.*, vol. 101, pp. 516–534, Feb. 2018.
[12] J. Yoon and J. Lee, "Effect of initial microstructure on Mg scroll forging under warm forming condition," *Mater. Trans.*, vol. 55, no. 2, pp. 238–244, Feb. 2014.
[13] H. Pashazadeh, J. Teimournezhad, and A. Masoumi, "Numerical investigation on the mechanical, thermal, metallurgical and material flow characteristics in friction stir welding of copper sheets with experimental verification," *Mater. Des.*, vol. 55, no. 4, pp. 619–632, Mar. 2014.
[14] W. Zeng and G. R. Liu, "Smoothed finite element methods (S-FEM): An overview and recent developments," *Arch. Comput. Methods Eng.*, vol. 25, no. 2, pp. 397–435, Apr. 2018.
[15] J. P. Song, Z. Y. Zhou, and Y. Q. Wu, "Tube transverse wall thickness of multimandrel mill," *Baosteel Technol.*, no. 6, pp. 39–41, 1997.
[16] B. M. Wang, *Hot Rolled Steel Tubes Quality*. Beijing, China: Metallurgical Industry Press of China, 1987, pp. 112–114.
[17] N. Khorshidi and A. Niazi, "A novel ion pair based surfactant assisted microextraction modified by orthogonal signal correction partial least squares for determination of food dyes," *J. Food Meas. Characterization*, vol. 12, no. 3, pp. 1885–1895, Sep. 2018.
[18] J. Zolgharnein, T. Shariatmanesh, and A. Babaei, "Simultaneous determination of propanil and monalide by modified glassy carbon electrode with nickel oxide nanoparticles, using partial least squares modified by orthogonal signal correction and wavelet packet transform," *Sens. Actuators B, Chem.*, vol. 197, no. 6, pp. 326–333, Jul. 2014.
[19] U. G. Indahl, "Towards a complete identification of orthogonal variation in multiple regression from a PLS1 modeling point of view: Including OPLS by a change of orthogonal basis," *J. Chemometrics*, vol. 28, no. 6, pp. 508–517, Jun. 2014.
[20] R. N. Feudale, H. Tan, and S. D. Brown, "Piecewise orthogonal signal correction," *Chemometrics Intell. Lab. Syst.*, vol. 63, pp. 129–138, Sep. 2002.
[21] R. Laref, D. Ahmadou, E. Losson, and M. Siadat, "Orthogonal signal correction to improve stability regression model in gas sensor systems," *J. Sensors*, vol. 2017, Aug. 2017, Art. no. 9851406.
[22] S. Wold, N. Kettaneh-Wold, and B. Skagerberg, "Nonlinear PLS modeling," *Chemometrics Intell. Lab. Syst.*, vol. 7, nos. 1–2, pp. 53–65, Dec. 1989.
[23] S. J. Qin, "Recursive PLS algorithms for adaptive data modeling," *Comput. Chem. Eng.*, vol. 22, nos. 4–5, pp. 503–514, 1998.
[24] J. Henseler, G. S. Hubona, and P. A. Ray, "Using PLS path modeling in new technology research: Updated guidelines," *Ind. Manage. Data Syst.*, vol. 116, no. 1, pp. 2–20, 2016.
[25] P. K. Wong, C. W. Hang, M. V. Chi, Z. Xie, and S. Huang, "Model predictive engine air-ratio control using online sequential extreme learning machine," *Neural Comput. Appl.*, vol. 27, no. 1, pp. 79–92, 2016.
[26] X. Luo *et al.*, "Towards enhancing stacked extreme learning machine with sparse autoencoder by correntropy," *J. Franklin Inst.*, vol. 355, no. 4, pp. 1945–1966, Mar. 2018.
[27] B. T. Le, D. Xiao, D. Okello, D. He, J. Xu, and T. Doan, "Coal exploration technology based on visible-infrared spectra and remote sensing data," *Spectrosc. Lett.*, vol. 50, no. 8, pp. 440–450, 2017.
[28] G.-B. Huang, "An insight into extreme learning machines: Random neurons, random features and kernels," *Cognit. Comput.*, vol. 6, no. 3, pp. 376–390, 2014.
[29] G. Huang, S. Song, J. N. D. Gupta, and C. Wu, "Semi-supervised and unsupervised extreme learning machines," *IEEE Trans. Cybern.*, vol. 44, no. 12, pp. 2405–2417, Dec. 2014.
[30] J. Cao, T. Chen, and J. Fan, "Fast online learning algorithm for landmark recognition based on BoW framework," in *Proc. 9th IEEE Conf. Ind. Electron. Appl.*, Hangzhou, China, Jun. 2014, pp. 1163–1168.
[31] X. Luo, C. Jiang, W. Wang, Y. Xu, J.-H. Wang, and W. Zhao, "User behavior prediction in social networks using weighted extreme learning machine with distribution optimization," *Future Gener. Comput. Syst.*, to be published, doi: 10.1016/j.future.2018.04.085.
[32] G. Feng, Z. Qian, and N. Dai, "Reversible watermarking via extreme learning machine prediction," *Neurocomputing*, vol. 82, pp. 62–68, Apr. 2012.
[33] Y. Yu, T.-M. Choi, and C.-L. Hui, "An intelligent quick prediction algorithm with applications in industrial control and loading problems," *IEEE Trans. Autom. Sci. Eng.*, vol. 9, no. 2, pp. 276–287, Apr. 2012.
[34] Y. Yang, Y. Wang, and X. Yuan, "Bidirectional extreme learning machine for regression problem and its learning effectiveness," *IEEE Trans. Neural Netw. Learn. Syst.*, vol. 23, no. 9, pp. 1498–1505, Sep. 2012.
[35] G.-B. Huang, D. H. Wang, and Y. Lan, "Extreme learning machines: A survey," *Int. J. Mach. Learn. Cybern.*, vol. 2, no. 2, pp. 107–122, Jun. 2011.
[36] J. Cao and L. Xiong, "Protein sequence classification with improved extreme learning machine algorithms," *BioMed Res. Int.*, vol. 2014, Mar. 2014, Art. no. 103054.
[37] L. L. C. Kasun, H. Zhou, G.-B. Huang, and C. M. Vong, "Representational learning with extreme learning machine for big data," *IEEE Intell. Syst.*, vol. 28, no. 6, pp. 31–34, Nov. 2013.
[38] G.-B. Huang, H. Zhou, X. Ding, and R. Zhang, "Extreme learning machine for regression and multiclass classification," *IEEE Trans. Syst., Man, Cybern. B, Cybern.*, vol. 42, no. 2, pp. 513–529, Apr. 2012.
[39] K. Javed, R. Gouriveau, and N. Zerhouni, "SW-ELM: A summation wavelet extreme learning machine algorithm with a *priori* parameter initialization," *Neurocomputing*, vol. 123, pp. 299–307, Jan. 2014.
[40] J. Cao, T. Chen, and J. Fan, "Landmark recognition with compact BoW histogram and ensemble ELM," *Multimedia Tools Appl.*, vol. 75, no. 5, pp. 2839–2857, Mar. 2016.
[41] D. P. Solomatine and D. L. Shrestha, "AdaBoost.RT: A boosting algorithm for regression problems," in *Proc. IEEE Int. Joint Conf. Neural Netw.*, Budapest, Hungary, Jul. 2004, pp. 1163–1168.

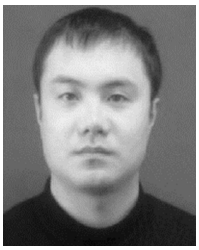

DONG XIAO received the Ph.D. degree in control theory and control engineering from Northeast University, Shenyang, China, in 2009.

Since 2006, he has been a Professor with the College of Information Science and Engineering, Northeast University. His research interests include neural networks, ELM algorithm, PLS algorithm, and MMMD algorithm.

FENGHUA YANG received the bachelor's degree in automation from Shandong Technology and Business University, Yantai, China, in 2016. Since 2016, he has been a Graduate Student with the College of Information Science and Engineering, Northeast University, Shenyang, China. His research direction is based on machine learning data processing. His research interests include convolution neural networks, image identification, and machine learning.

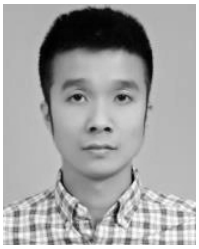

BA TUAN LE was born in Phu Tho, Vietnam. He is currently pursuing the Ph.D. degree with the College of Information Science and Engineering, Northeastern University, China. His area of interests includes intelligence information process, remote sensing exploration, and spectral analysis technique.

SHENGYONG ZHANG received the bachelor's degree in automation from Northeast University, Shenyang, China, in 2016.

Since 2016, he has been a Graduate Student with the College of Information Science and Engineering, Northeast University. His research direction is based on machine learning and data processing. His research interests include neural networks, ELM algorithm, and machine learning.